JPn Neuroscience
The Journal of Physiology

Parallel processing of afferent olfactory sensory information

Christopher E. Vaaga[1,2] and Gary L. Westbrook[1]

[1] *Vollum Institute*
[2] *Neuroscience Graduate Program, Oregon Health and Science University, Portland, OR, USA*

Key points

- The functional synaptic connectivity between olfactory receptor neurons and principal cells within the olfactory bulb is not well understood.
- One view suggests that mitral cells, the primary output neuron of the olfactory bulb, are solely activated by feedforward excitation.
- Using focal, single glomerular stimulation, we demonstrate that mitral cells receive direct, monosynaptic input from olfactory receptor neurons.
- Compared to external tufted cells, mitral cells have a prolonged afferent-evoked EPSC, which serves to amplify the synaptic input.
- The properties of presynaptic glutamate release from olfactory receptor neurons are similar between mitral and external tufted cells.
- Our data suggest that afferent input enters the olfactory bulb in a parallel fashion.

Abstract Primary olfactory receptor neurons terminate in anatomically and functionally discrete cortical modules known as olfactory bulb glomeruli. The synaptic connectivity and postsynaptic responses of mitral and external tufted cells within the glomerulus may involve both direct and indirect components. For example, it has been suggested that sensory input to mitral cells is indirect through feedforward excitation from external tufted cells. We also observed feedforward excitation of mitral cells with weak stimulation of the olfactory nerve layer; however, focal stimulation of an axon bundle entering an individual glomerulus revealed that mitral cells receive monosynaptic afferent inputs. Although external tufted cells had a 4.1-fold larger peak EPSC amplitude, integration of the evoked currents showed that the synaptic charge was 5-fold larger in mitral cells, reflecting the prolonged response in mitral cells. Presynaptic afferents onto mitral and external tufted cells had similar quantal amplitude and release probability, suggesting that the larger peak EPSC in external tufted cells was the result of more synaptic contacts. The results of the present study indicate that the monosynaptic afferent input to mitral cells depends on the strength of odorant stimulation. The enhanced spiking that we observed in response to brief afferent input provides a mechanism for amplifying sensory information and contrasts with the transient response in external tufted cells. These parallel input paths may have discrete functions in processing olfactory sensory input.

(Received 5 May 2016; accepted after revision 22 June 2016; first published online 5 July 2016)
Corresponding author G. L. Westbrook: L474, Vollum Institute, 3181 SW Sam Jackson Park Road, Portland, OR 97239, USA. Email: westbroo@ohsu.edu

Abbreviations ChR2, channelrhodopsin-2; CPCCOEt, 7-(hydroxyimino)cyclopropa[*b*]chromen-1a-carboxylate ethyl ester; NBQX, 2,3-dioxo-6-nitro-1,2,3,4-tetrahydrobenzo[f]quinoxaline-7-sulphonamide; ORN, olfactory receptor neuron; p, postnatal day; (*R*)-CPP, 3-((*R*)-2-carboxypiperazin-4-yl)-propyl-1-phosphonic acid; WT, wild-type; YFP, yellow fluorescent protein.

DOI: 10.1113/JP272755

Introduction

The olfactory bulb is organized into anatomically and functionally discrete cortical modules known as glomeruli. Each glomerulus receives afferent sensory innervation from olfactory receptor neurons (ORNs) expressing the same odorant receptor from a large multigene family (Buck and Axel, 1991; Vassar *et al.* 1993; Ressler *et al.* 1994; Mombaerts *et al.* 1996, Treloar *et al.* 2002). Therefore, the spatial map of activated glomeruli across the olfactory bulb surface is representative of odorant identity (Mori *et al.* 1999; Rubin and Katz, 1999; Wachowiak and Cohen, 2001). Principal neurons send their dendrites to a single glomerulus, thereby preserving the one-to-one connectivity. Principal neurons are broadly categorized as mitral cells and tufted cells, with tufted cells further divided into internal, middle and external tufted cells depending on the position of their cell body (Pinching and Powell, 1971*b*).

Recent studies suggest that external tufted cells play a major role in processing incoming olfactory sensory information. External tufted cells co-ordinate neuronal elements by providing feedforward excitation to intrinsic interneurons, as well as drive activity in mitral/tufted cells, through chemical synapses and electrical coupling (Hayar *et al.* 2004; De Saint Jan *et al.* 2009; Najac *et al.* 2011). In the present study, we define feedforward excitation as a circuit in which ORNs directly activate external tufted cells, which, in turn, activate mitral cells. This feedforward circuit arrangement has been proposed as the sole means of activating mitral cells (Gire and Schoppa, 2009; Gire *et al.* 2012; but see also De Saint Jan and Westbrook, 2007; De Saint Jan *et al.* 2009; Najac *et al.* 2011). In this view, mitral cells respond to sensory input via slow disynaptic responses mediated solely by dendrodendritic synapses (Carlson *et al.* 2000; Schoppa and Westbrook, 2001; De Saint Jan and Westbrook, 2007; De Saint Jan *et al.* 2009; Gire and Schoppa, 2009; Gire *et al.* 2012). Although early ultrastructural evidence indicates ORN axon terminals contact mitral cell dendrites (Pinching and Powell, 1971*a*; White, 1973; Kosaka *et al.* 2001), it remains a matter of controversy whether mitral cells receive physiologically relevant input from ORN axon terminals (De Saint Jan *et al.* 2009; Gire and Schoppa 2009; Najac *et al.* 2011; Gire *et al.* 2012). This is an important issue because mitral cells constitute the majority of principal neurons innervating the glomerular layer, and project extensively to areas of higher olfactory cortex (Igarashi *et al.* 2012).

To address this question, we used focal stimulation of axon bundles innervating single glomeruli to probe the synaptic connectivity between ORN terminals and their glomerular targets. Whole cell recordings from mitral and external tufted cells showed that both cell types receive unambiguous, direct afferent input; however, stimulating fewer afferents with diffuse stimulation in the olfactory nerve layer produced slow, polysynaptic currents in mitral cells. In response to focal stimulation, the synaptic charge was substantially larger in mitral cells than in external tufted cells. Despite these differences in postsynaptic responses, the paired pulse ratio (an indicator of presynaptic release probability) and the quantal amplitude were similar in both cell types. The distinct properties of external tufted and mitral cell responses to afferent stimuli indicate that glomerular processing involves the integration of these two pathways. Furthermore, whether a mitral cell shows monosynaptic or polysynaptic, or both, responses will depend on the relative number of activated afferent fibres.

Methods

Animals

We used adult male and female mice [postnatal day (p)21–p42] from wild-type (WT) C57Bl6/J mice, as well as three transgenic mouse strains: Tg(Thy1-YFP)GJrs heterozygous mice, $Cx36^{-/-}$;$mGluR2\text{-}GFP^{+/-}$ mice, and OMP-cre;Rosa26(lsl-ChR2-YFP) mice. The Tg(Thy1-YFP)GJrs (Thy1-YFP mice) (Feng *et al.* 2000) mice were on a mixed C57Bl6/CBA background, which did not alter the physiological or morphological properties of neurons within the olfactory bulb (Bartel *et al.* 2015). Thus, experiments from both genetic backgrounds were grouped, where appropriate. The Oregon Health and Science University Institutional Animal Care and Use Committee (IACUC) approved all animal use and procedures.

Slice preparation

Olfactory bulb slices were obtained as described previously (Schoppa and Westbrook, 2001). Briefly, animals were anaesthetized with an I.P. injection of 2% avertin (2, 2, 2-tribromoethanol), and transcardially perfused with 10 ml of 4°C sucrose-based cutting solution oxygenated with 95% O_2 and 5% CO_2 followed by decapitation. The cutting solution contained (in mM): 83 NaCl, 2.5 KCl, 1 NaH_2PO_4, 26.2 $NaHCO_3$, 22 dextrose, 72 sucrose, 0.5 $CaCl_2$ and 3.3 $MgSO_4$ (300–310 mosmol, pH 7.3). The brain was removed and coronally blocked at the level of the striatum. Horizontal sections (250 μm) were cut using a 1200 s vibratome (Leica Microsystems, Wetzlar, Germany). Sections were recovered for 20–30 min in 34–36°C artificial cerebrospinal fluid, which contained (in mM): 125 NaCl, 25 $NaHCO_3$, 1.25 NaH_2PO_4, 3 KCl, 2.5 dextrose, 2 $CaCl_2$ and 1 $MgCl_2$ (300–310 mosmol, pH 7.3). Sections were stored in artificial cerebrospinal fluid at room temperature until they were transferred to the recording chamber.

Electrophysiology

Whole cell voltage clamp and current clamp recordings were made from mitral cells and external tufted cells under visual control using differential interference contrast optics and an ORCA II camera system (Hamamatsu Corp., Bridgewater, NJ, USA). Patch pipettes (3–4 MΩ) contained (in mM): 130 K-gluconate, 20 KCl, 10 Hepes, 0.1 EGTA, 4 MgATP, 0.3 NaGTP and 0.07–0.1 Alexa-594 hydrazide (osmolality adjusted to 295, pH adjusted to 7.21 with KOH). The liquid junction potential of the internal solution was −7 mV and was not corrected. The sodium channel blocker QX-314-Cl (5 mM) was included in the patch pipette for voltage clamp experiments to block unclamped action potentials. To record NMDA receptor responses, a cesium based internal was used, which included (in mM): 113 CsGluconate, 10 Hepes, 10 EGTA, 17.5 CsCl, 8 NaCl, 2 MgATP and 0.3 NaGTP (osmolality adjusted to 290, pH adjusted to 7.3 with CsOH). All recordings were performed at 32–34°C. Data were acquired using a Multiclamp 700B amplifier (Molecular Devices, Sunnyvale CA, USA) and Axograph X acquisition software (http://www.axograph.com). Data were low-pass Bessel filtered at 4 kHz and digitized at 10 kHz. The series resistance, generally <10 MΩ for mitral cells and <25 MΩ for external tufted cells, was not compensated. Series resistance was continuously monitored with a −10 mV hyperpolarizing step. Cells with >30% change in series resistance were excluded from analysis. Unless otherwise noted, for all voltage clamp experiments, the holding potential was −70 mV. For current clamp experiments, a hyperpolarizing bias current (usually <200 pA) was injected to maintain the membrane voltage at −60 ± 5 mV.

Mitral cells and external tufted cells were identified morphologically as described previously (Pinching and Powell 1971*a*; Hayar *et al.* 2004). Mitral cells were identified by their soma position within the mitral cell layer, the presence of a single apical dendrite innervating a glomerulus, as well as lateral dendrites extending into the external plexiform layer. Mitral cells had an average input resistance of 63.8 ± 5.1 MΩ (minimum 32 MΩ, maximum 130 MΩ, $n = 25$ cells). External tufted cells were identified by their pear-shaped, large cell bodies located within the outer one-third of the glomerular layer. External tufted cells were further distinguished from juxtaglomerular interneurons by the presence of a thick apical tuft ramifying into a single glomerulus and the lack of lateral dendrites (Kiyokage *et al.* 2010). The average input resistance of external tufted cells was 225.3 ± 19.5 MΩ (minimum 52 MΩ, maximum 477 MΩ, $n = 40$ cells). We also used yellow fluorescent protein (YFP) expression in the Thy1-YFP transgenic line, which labelled both cell types. All cells were filled with Alexa-594 during the recording, allowing for the identification of both cell type and dendritic targeting.

EPSCs were evoked using a constant voltage stimulator (100 μs, 5–100 V) in conjunction with a small-bore theta glass electrode (theta electrode) filled with 2 M NaCl, or with a bipolar electrode placed in the olfactory nerve layer. The tip diameter of the theta electrode (1–2 μm), provided precise, spatial stimulation because ORN axons innervating a glomerulus fasciculate into tight bundles just prior to entering the glomerulus (Mombaerts *et al.* 1996; De Saint Jan *et al.* 2009; Borisovska *et al.* 2011; Najac *et al.* 2011). Although the stimulation voltage used for the theta electrode appears to be high, the effective current is greatly attenuated by the high impedance of the theta electrode, especially at higher intensities. All recordings were performed on the medial aspect of the olfactory bulb, where the ORN bundle topography is better defined. Recordings were only made if the innervated glomerulus was near the slice surface with a visibly identifiable ORN axon bundle entering from the olfactory nerve layer. Theta electrodes were placed within 20–30 μm of the glomerulus border to avoid stimulating fibres of passage. It is worth noting that our stimulation did not saturate responses, indicating that we were not stimulating every axon in a bundle. In optogenetic stimulation experiments, 2 ms wide-field LED illumination was centered at the glomerulus containing the apical dendrite of the recorded cell.

All drugs were bath applied to the slice via a recirculating pump. The drugs included: 10 μM 2,3-dioxo-6-nitro-1,2,3,4-tetrahydrobenzo[*f*]quinoxaline-7-sulphonamide (NBQX) to block AMPA receptors, 5–10 μM 3-((*R*)-2-carboxypiperazin-4-yl)-propyl-1-phosphonic acid [(*R*)-CPP] to block NMDA receptors, 20 μM 7-(hydroxyimino)cyclopropa[*b*]chromen-1a-carboxylate ethyl ester (CPCCOEt) to block mGluR1 receptors and 3 mM strontium chloride to desynchronize vesicle release. All drugs were purchased from either Tocris Biosciences (Ellisville, MO, USA) or Ascent Scientific (Bristol, UK).

Imaging

Validation of the channelrhodopsin-2 (ChR2) expression patterns following the OMP-cre;Ai32 genetic cross was performed on a LSM 780 confocal microscope (Carl Zeiss, Oberkochen, Germany). Briefly, animals were deeply anaesthetized with 2% avertin (2, 2, 2-tribromoethanol) then transcardially perfused with 4% paraformaldehyde followed by a 24 h drop fixation. The tissue was then sectioned (100 μm) on a vibratome. Intrinsic ChR2-YFP expression was boosted with a 488-conjugated secondary antibody (rabbit anti-GFP 488; 2 h, room temperature).

Before mounting onto glass a slide, the tissue was counter-stained with 4′,6-diamidino-2-phenylindole (dilution 1:10,000; Sigma-Aldrich, St Louis, MO, USA).

Data analysis

Electrophysiological data were analysed in Axograph X or imported into IGOR Pro, version 6.22A (WaveMetrics, Inc., Lake Oswego, OR, USA). Confocal data were analysed and prepared in ImageJ (https://imagej.nih.gov). Unless otherwise noted, all voltage clamp traces represent the average of 10 sweeps after baseline subtraction. Peak EPSC amplitude, 10% onset time, peak location and charge transfer were calculated using built-in routines in Axograph X. The total charge transfer was calculated by integrating the current until the EPSC amplitude recovered to 10% of the original peak amplitude (time to 90% recovery). For current clamp recordings, action potentials were detected using a threshold criterion (0 mV) in Axograph X. The total number of spikes in each trial, as well as the latency to the first spike, was calculated and then averaged across trials. To measure the time course of AMPA receptor block in paired recordings, a sigmoidal curve was fit to a diary plot of normalized peak EPSC amplitudes using a built-in Igor routine. The time at half-maximal (x_{half}) block was recorded and averaged across cells. Quantal EPSC events were detected using an Axograph X scanning template, consisting of a single exponential (−30 pA amplitude, 0.5 ms rise time, 2 ms decay time constant). Miniature EPSCs were manually reviewed and any events with half-widths >2 ms were excluded to prevent GABAergic contamination. AMPA/NMDA ratios were calculated using fast AMPA receptor amplitudes at −70 mV and NMDA receptor amplitudes at +40 mV (at 50 ms post-stimulus).

Statistical analysis

All data are reported as the mean ± SE unless otherwise noted. Statistical analyses were performed in Prism, version 6 (GraphPad Software Inc., La Jolla, CA, USA). Unless otherwise noted, data were considered as normally distributed and analysed using a paired or unpaired Student's *t* test as appropriate. For sequential drug application experiments and paired pulse ratio experiments, a one-way repeated measure ANOVA was used with a Holm–Sidak's multiple comparison *post hoc* test. We used two-way repeated measure ANOVAs for experiments in which the responses to increasing stimulus intensity were compared, and in which the repeated measures represented cell type and stimulus intensity. To determine a cell type interaction, a Holm–Sidak *post hoc* test was used to compare mitral cell and external tufted cell responses at a given stimulus intensity. In non-parametric data sets, Mann–Whitney rank comparison tests were used to assess significance. In all experiments, α was set to $P < 0.05$.

Results

Single glomerulus stimulation evoked a monosynaptic afferent response in mitral cells

The current view that mitral cells receive indirect, polysynaptic input from external tufted cells is based on peri-threshold stimulation in the olfactory nerve layer, designed to avoid directly stimulating dendritic glutamate release (Gire and Schoppa 2009; Gire *et al.* 2012). With weak distal bipolar stimulation of the olfactory nerve layer (bipolar electrode placed six to ten glomeruli anterior to target glomerulus), we also observed a slow current in mitral cells (peak amplitude: 96.9 ± 21.0 pA; time-to-peak: 489.8 ± 106.1 ms post stimulus, $n = 5$ cells) without a significant fast current (peak amplitude measured within 6 ms: 32.7 ± 13.1 pA; one-sample *t* test: $P = 0.066$) (Fig. 1*A* and *B*). In the same cells, however, focal theta electrode stimulation of an ORN bundle innervating a single glomerulus produced a biphasic EPSC with a prominent fast component (fast peak amplitude: 355.96 ± 59.4 pA, $P = 0.005$; time-to-peak: 4.2 ± 0.2 ms, one-sample *t* test: $P = 0.004$, paired Student's *t* test: $P = 0.01$, $n = 5$ cells) (Fig. 1*A* and *B*).

To ensure that the fast current elicited with theta electrode stimulation was not an artefact of directly stimulating glutamate release from mitral cell dendrites (Schoppa and Westbrook, 2001; Urban and Sakmann, 2002; De Saint Jan and Westbrook, 2007; Najac *et al.* 2011), which is a primary concern when using this stimulation technique, we placed the bipolar electrode more proximal to the target glomerulus (two to three glomeruli anterior to the innervated glomerulus) within the olfactory nerve layer. Bipolar stimulation (30–80 V) elicited biphasic EPSCs in mitral cells, which were indistinguishable from EPSCs elicited with the theta electrode (bipolar fast peak amplitude: 495.3 ± 33.5 pA, theta fast peak amplitude: 356.0 ± 59.4 pA, $P = 0.08$; bipolar time-to-peak: 4.8 ± 0.8 ms, theta time-to-peak: 4.2 ± 0.2 ms, $P = 0.52$, $n = 5$ cells each group) (Fig. 1*C* and *D*). Taken together, these data strongly suggest that the monosynaptic current elicited with the theta electrode is not a result of dendritic glutamate release, and further suggest that the relative contributions of the slow and fast currents in mitral cells differ depending on the number of afferents stimulated.

To characterize the spatial spread of stimulation using the theta electrode, mitral cells were filled with Alexa-594, which provided direct identification of the glomerulus innervated by the apical dendrite. When the theta electrode was placed in the centre of the ORN bundle ∼30–50 μm from the edge of the glomerulus (Fig. 2*A* and *B*), brief

stimulation (0.1 ms) elicited a large, two-component EPSC in all mitral cells examined ($n = 6$ cells). With lateral movement of the theta electrode (10 μm steps), the fast EPSC decayed with a space constant of 11.4 μm (Fig. 2*C* and *D*) and was almost abolished at 30 μm (7.0 $\pm$ 5.4% of control), indicating that focal stimulation was limited to the diameter of the axon bundle and probably did not spread to the dendritic arbor of principal neurons within the glomerulus. We next made paired recordings of external tufted cells innervating neighbouring glomeruli separated by at most a single intervening glomerulus (Fig. 2*E*). Stimulation in the 'target' glomerulus evoked a large amplitude EPSC (0.9 $\pm$ 0.2 nA; $n = 12$ cells, $n = 6$ pairs) (Fig. 2*F*) but failed to elicit an EPSC in cells projecting to the neighbouring or 'off target' glomerulus (6.9 $\pm$ 1.7 pA; $n = 12$ cells, $n = 6$ pairs; $P = 0.0012$) (Fig. 2*F*). In all pairs, moving the theta electrode to the other glomerulus reversed these results (Fig. 2*F*). Taken together, these data suggest that the theta electrode stimulation produced spatially restricted, single glomerulus stimulation.

To determine whether the fast component of the EPSC in mitral cells results from a monosynaptic connection, we stimulated the ORN while monitoring synaptic latency and jitter. Monosynaptic EPSCs are characterized by their short latency (<2 ms) and low synaptic jitter (Berry and Pentreath, 1976). Using theta electrode stimulation at 5 Hz, EPSCs in both mitral cells and external tufted cells showed a short synaptic latency (mitral cell: 1.5 $\pm$ 0.07 ms, $n = 5$ cells; external tufted cell: 1.7 $\pm$ 0.01 ms, $n = 4$ cells; $P = 0.27$) (Fig. 3*A* and *B*). Similarly, the synaptic jitter (standard deviation of the EPSC onset times) was not significantly different between mitral cells and external tufted cells (mitral cell: 0.08 $\pm$ 0.004, $n = 5$ cells; external tufted cell: 0.07 $\pm$ 0.007, $n = 4$ cells; $P = 0.18$) (Fig. 3*A* and *B*). These latencies are consistent with monosynaptic chemical transmission following axonal stimulation and strongly suggest that both cell types receive monosynaptic input from the olfactory nerve.

If mitral cells only received input from feedforward excitation by external tufted cells, then block of feed-forward excitation with an AMPA receptor antagonist should prevent an EPSC in mitral cells. As expected, application of NBQX (10 μM) almost abolished the ORN-evoked EPSC in external tufted cells by (3.4 $\pm$ 0.8% of control; control: 1.3 $\pm$ 0.3 nA; NBQX: 0.05 $\pm$ 0.01 nA; $n = 4$ cells; $P = 0.02$). However, a monosynaptic EPSC in mitral cells was still present as measured by the NMDA receptor current at positive membrane potentials (V_H +70 mV: 212.9 $\pm$ 61.7 pA; $n = 7$ cells) (Fig. 3*C*), which was blocked by bath application of the NMDA receptor antagonist, R-CPP (5–10 μM; 5.6 $\pm$ 1.5% of control;

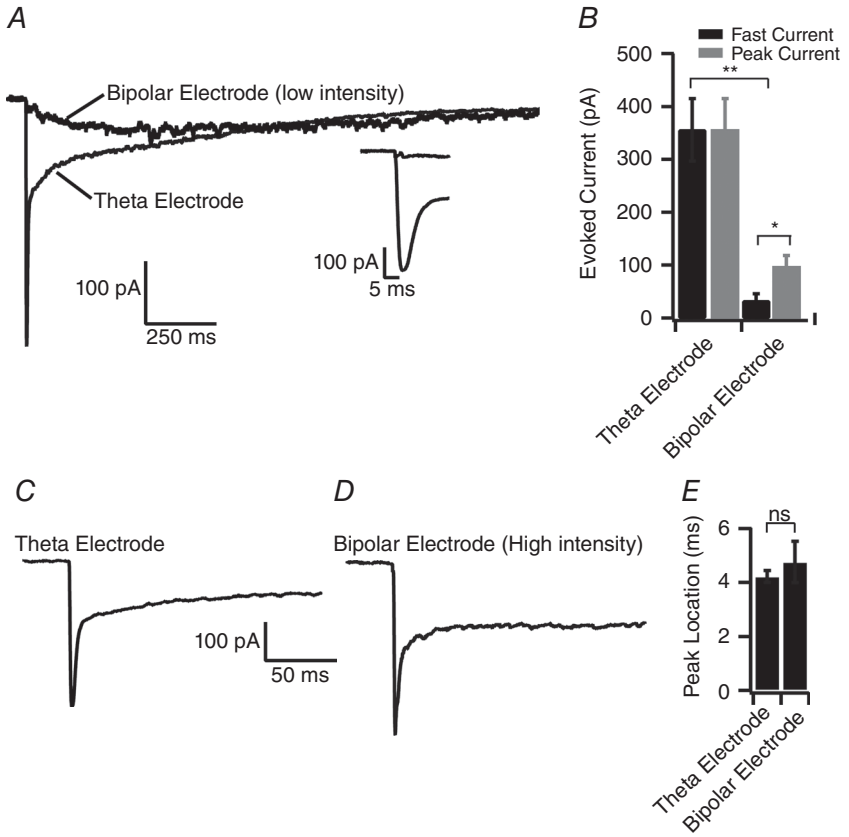

Figure 1. Comparing diffuse and focal stimulation
A, comparison of synaptic responses recorded in single mitral cells following either bipolar electrode stimulation or theta electrode stimulation (stimulus location indicated by black arrowhead). For bipolar stimulation, the electrode was placed six to 10 glomeruli anterior to the target glomerulus in the olfactory nerve layer (stimulus intensity: 10–40 V). Conversely, for theta electrode stimulation, the electrode was placed in the centre of the axon bundle entering the glomerulus. Inset: lack of a fast current following bipolar stimulation. *B*, comparison of the fast EPSC amplitude (measured within 6 ms of the stimulus) and the peak EPSC. For theta electrode stimulation, the peak EPSC occurred within 6 ms of the stimulus, however, for bipolar stimulation, the peak EPSC occurred 489.9 $\pm$ 106.1 ms after the stimulus. *C* and *D*, comparison of mitral cell responses to theta electrode and proximal bipolar electrode stimulation. The bipolar electrode was placed closer to the target glomerulus (3-5 glomeruli anterior; stimulus intensity: 30–80 V). Both stimulation paradigms elicited a biphasic EPSC waveform. *E*, comparison of the time-to-peak for bipolar and theta electrode stimulation.

$P = 0.017$) (Fig. 3*C* and *D*). The NMDA receptor current had a rise time of 6.9 ± 4.7 ms and a latency of 2.9 ± 0.2 ms, which is consistent with the slow activation kinetics of synaptic NMDA receptors. Furthermore, if mitral cells and external tufted cells receive monosynaptic input, the rate of AMPA receptor antagonist block should be similar across both cell types. In paired mitral and external tufted cell recordings, bath application of NBQX reduced the ORN-evoked EPSC in parallel (time to half-maximal response amplitude: mitral cell: 125.3 ± 8.9 s; external tufted cell: 129.1 ± 8.4 s; paired Student's *t* test: $P = 0.79$, NBQX block: mitral cell: 5.9 ± 5.3% of control; external tufted cell: 4.7 ± 1.2% of control, paired Student's *t* test: $P = 0.79$, $n = 4$ pairs).

To further validate that the fast current elicited by theta electrode stimulation was not a result of dendritic glutamate release, we also compared activation of mitral and external tufted cells using optical stimulation. Using an OMP-cre;Rosa26(lsl-hChR2-YFP) mouse that expresses the light activated channelrhodopsin selectively in olfactory receptor neurons (Fig. 4*A*), 2 ms optical stimulation (Fig. 4*B*) elicited a fast EPSC in both mitral and external tufted cells (mitral cell: 1.2 ± 0.2 nA, $n = 7$ cells; external tufted cell: 1.9 ± 0.6 nA, $n = 7$ cells)

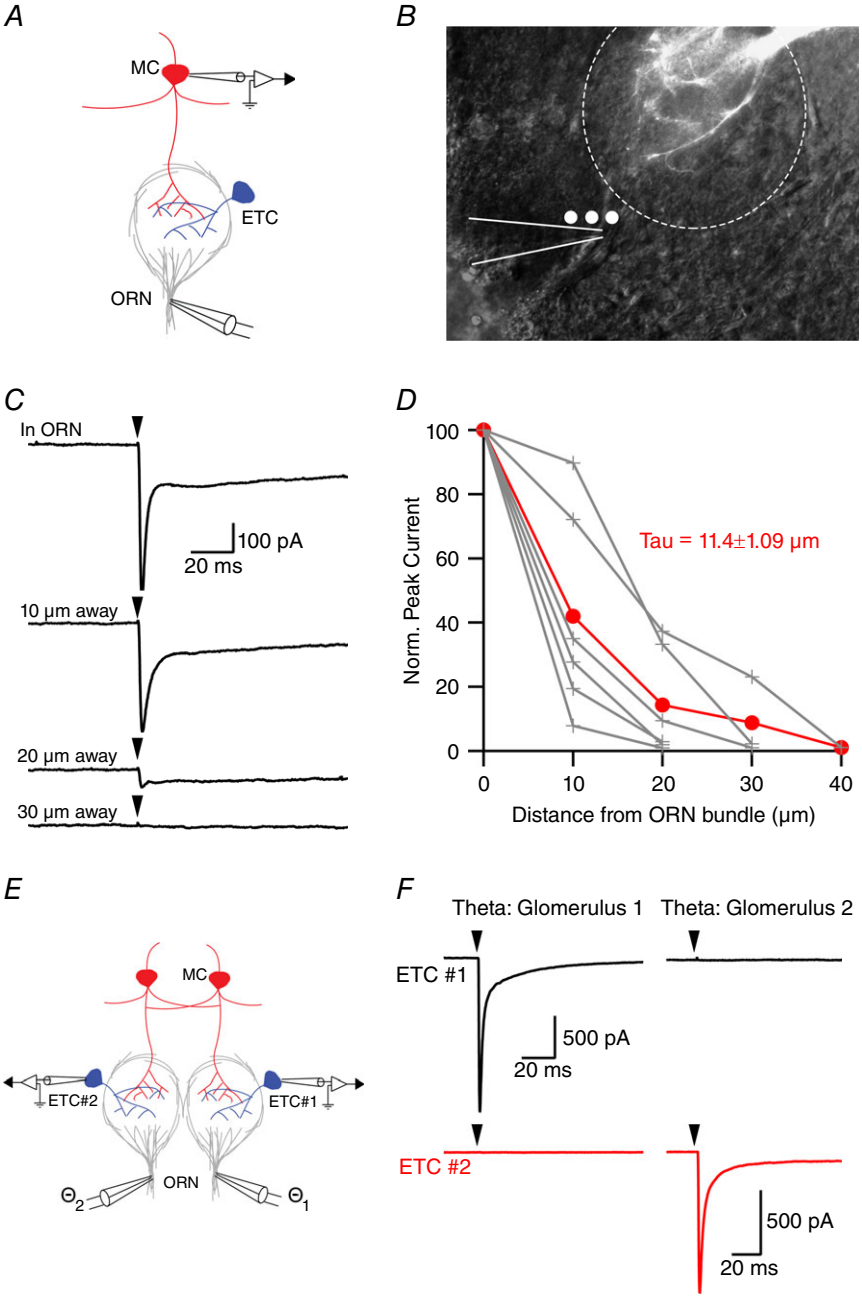

Figure 2. Single glomerulus stimulation using theta glass electrodes
A, schematic of recording configuration. A two-barreled glass theta electrode with a tip diameter of 1–2 µm was placed in the centre of a visibly identifiable ORN axon bundle just prior to entering a glomerulus. *B*, mitral cell apical dendrite filled with Alexa-594 dye innervating the depicted glomerulus. Theta electrode (outlined in white) placement in an ORN bundle entering the innervated glomerulus. White dots represent ~10 µm steps laterally from the ORN bundle. *C* and *D*, theta electrode stimulation elicited biphasic EPSCs when the theta electrode was placed in the centre of the ORN bundle (arrowheads indicate the time of stimulation). Moving the theta electrode laterally resulted in a rapid attenuation of the peak EPSC with a space constant of 11.4 ± 1.09 µm ($n = 6$ cells). *E*, paired external tufted cell recording configuration with each cell innervating distinct glomeruli. *F*, stimulation of the 'target' glomerulus produced a large EPSC in the corresponding external tufted cell but failed to produce an EPSC in the external tufted cell innervating the 'neighbouring' glomerulus. MC, mitral cell; ETC, external tufted cell. [Colour figure can be viewed at wileyonlinelibrary.com]

(Fig. 4*C* and *D*). Compared to electrical stimulation, optical stimulation elicited larger fast currents, probably reflecting the optical activation of more ORN fibres. Furthermore, although the synaptic latency and jitter from optical stimulation were longer than electrical stimulation as a result of the intrinsically slower kinetics of channelrhodopsin, there were no statistically significant differences in the synaptic latency or jitter across the two cell types (latency: mitral cell: 5.2 ± 0.2 ms, external tufted cell: 5.0 ± 0.5 ms, $P = 0.73$; jitter: mitral cell: 0.2 ± 0.04, external tufted cell: 0.2 ± 0.04, $P = 0.78$). The fast component of the optically-stimulated EPSC in mitral cells indicates that the response results from monosynaptic input from olfactory nerve axons and not from dendritic glutamate release.

Mitral cells and external tufted cells differentially respond to afferent input

It is well know that afferent stimulation causes a long lasting depolarization in mitral cells (Carlson *et al.* 2000; Schoppa and Westbrook, 2001), which is mediated, in part, by NMDA receptor-dependent dendritic release of glutamate (Nicoll and Jahr, 1982; Aroniadou-Anderjaska *et al.* 1999; Carlson *et al.* 2000; Christie and Westbrook, 2006; De Saint Jan and Westbrook, 2007; Pimentel and Margrie, 2008; Najac *et al.* 2011). Theta electrode stimulation also elicited a biphasic EPSC in mitral cells, with a prominent slow component. The monosynaptic currents in both mitral and external tufted cells are larger than reported elsewhere (mitral cell: 322.8 ± 25.4 pA; external tufted cell: 3.1 ± 0.8 nA); however, this larger amplitude reflects the stimulation of more axons using the focal, theta electrode stimulation. In mitral cells, the ORN-evoked EPSC duration was 1014.1 ± 126.5 ms ($n = 8$ cells), whereas stimulation elicited a much faster EPSC in external tufted cells (EPSC duration: 27.7 ± 6.9 ms, $n = 6$ cells; $P < 0.001$). To compare the fractional contribution of the slow component, we measured the amplitude of the slow current at 200 ms post-stimulus. This amplitude was 125.8 ± 26.3 pA or 39.5 ± 3.3% of the peak EPSC in mitral cells ($n = 8$) compared to 27.9 ± 40.6 pA or 0.8 ± 0.5% of the peak EPSC in external tufted cells ($n = 6$; unpaired Student's *t* test: $P = 0.013$). Therefore, although a small slow current is present in external tufted cells, the relative contribution of this current to the EPSC is much smaller than in mitral cells.

We next compared the receptor profiles of the two EPSCs by sequentially blocking NMDA, mGluR1 and AMPA receptors. In mitral cells, bath application of CPP reduced the synaptic charge to 24.5 ± 1.1% of control (control: 99.2 ± 8.4 pC; CPP: 24.3 ± 1.1 pC; Holm–Sidak *post hoc* test: $P < 0.05$; $n = 8$ cells) (Fig. 5*A* and *B*) without altering the fast peak EPSC amplitude (control: 322.8 ± 25.4 pA; CPP: 286.3 ± 16.5 pA; Holm–Sidak *post hoc* test: $P > 0.05$) (Fig. 5*A*, inset and *C*). Addition of CPCCOEt further reduced the synaptic charge to 9.9 ± 0.6% of control (CPP/CPCCOEt: 9.9 ± 0.6 pC; Holm–Sidak *post hoc* test: $P < 0.05$) (Fig. 4*A* and *B*) and NBQX abolished the synaptic charge (0.6 ± 0.2% of control; CPP/CPCCOEt/NBQX: 0.6 ± 0.2 pC; Holm–Sidak *post hoc* test: $P < 0.01$) (Fig. 5*A* and *B*) and the peak EPSC amplitude (1.8 ± 0.4% of control; −5.9 ± 1.3 pA; Holm-Sidak *post hoc* test: $P < 0.01$) (Fig. 5*A*, inset and *C*).

By contrast, bath application of CPP in external tufted cells only produced a non-significant decrease in synaptic charge (control: 26.4 ± 8.1 pC; CPP: 18.4 ± 5.4 pC; Holm–Sidak *post hoc* test: $P > 0.05$; $n = 6$ cells) (Fig. 5*D* and *E*) and CPCCOEt had no effect on the synaptic charge (CPP/ CPCCOEt: 17.8 ± 5.1 pC; Holm–Sidak *post hoc* test: $P > 0.05$) (Fig. 5*D* and *E*). As in mitral cells, CPP had no effect on the fast peak EPSC amplitude (92.3 ± 10.5% of control; Holm–Sidak *post hoc* test: $P > 0.05$) (Fig. 5*D*, inset and *F*). Consistent with the AMPA receptors producing the majority of the external tufted cell EPSC, NBQX reduced

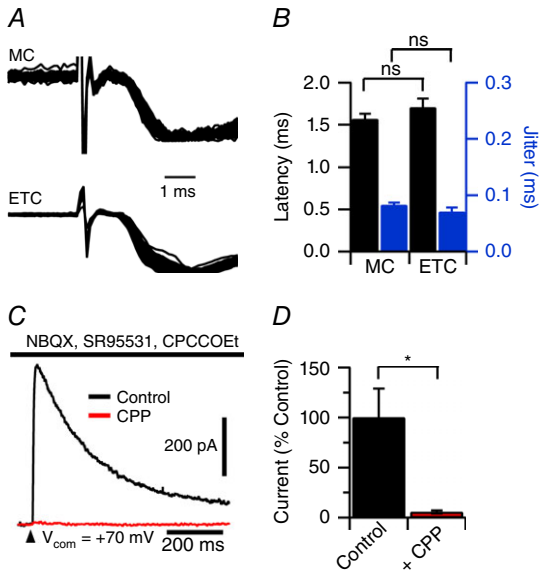

Figure 3. Monosynaptic EPSC in mitral cells, not just external tufted cells
A and *B*, overlay of 50 sweeps recorded in mitral cells and external tufted cells (100 V theta stimulation) demonstrating the short synaptic latency and low synaptic jitter typical of a monosynaptic connection. In mitral cells, NMDA and mGluR1 receptor antagonists (10 μM CPP and 20 μM CPCCOEt, respectively) were included to isolate the AMPA receptor-mediated current. Responses in both cells were peak scaled. The synaptic latency was measured as the time to 10% of the peak EPSC response. *C* and *D*, block of feedforward excitation with AMPA receptor antagonists (10 μM NBQX) failed to block an NMDA receptor-mediated EPSC in mitral cells when held at positive potentials. The ORN-evoked NMDA-receptor EPSC was blocked by bath application of CPP (10–20 μM). GABA and mGluR1 receptor antagonists (SR95531, 10 μM and CPCCOEt, 20 μM) were also included. [Colour figure can be viewed at wileyonlinelibrary.com]

the synaptic charge to 2.1 ± 0.4% of control (control: 26.4 ± 8.1 pC; NBQX: 0.6 ± 0.3 pC; Holm–Sidak *post hoc* test: $P < 0.05$) (Fig. 5*D* and *E*) and the peak amplitude to 0.8 ± 0.1% of control (control: 3.1 ± 0.9 nA; NBQX: 0.02 ± 0.006 nA; Holm–Sidak *post hoc* test: $P < 0.05$) (Fig. 5*D*, inset and *F*). These data demonstrate the vastly different kinetic and pharmacological profiles of the two monosynaptic EPSCs.

The slow component of the mitral cell EPSC is considered to result from the NMDA receptor-dependent dendritic glutamate release and not from NMDA receptors apposing afferent nerve terminals (Nicoll and Jahr, 1982; Aroniadou-Anderjaska *et al.* 1999; Isaacson, 1999; Carlson *et al.* 2000; Friedman and Strowbridge, 2000; Christie *et al.* 2001; Schoppa and Westbrook, 2001; De Saint Jan and Westbrook, 2007). We tested this directly in $Cx36^{-/-}$ mice, which eliminates dendrodendritic release (Christie *et al.* 2005; Christie and Westbrook, 2006; Maher *et al.* 2009; Gire *et al.* 2012). The AMPA/NMDA ratio did not differ between mitral cells (4.67 ± 0.27, $n = 7$ cells) (Fig. 5*G* and *I*) and external tufted cells (4.49 ± 0.82, $n = 7$ cells; $P = 0.83$) (Fig. 5*H* and *I*), indicating that the complement of postsynaptic receptors at afferent synapses within the shell of the glomerulus does not explain the different EPSC timecourses.

Paired recording of mitral and external tufted cells

To directly compare responses to afferent stimulation, we recorded from pairs of mitral and external tufted cells innervating the same glomerulus at a variety of stimulus intensities (Fig. 6*A* and *B*). As shown in the stimulus-evoked input–output curve, external tufted cells had a larger fast EPSC amplitude at all stimulus intensities (amplitude at 100 V: external tufted cell: 3.0 ± 0.6 nA; mitral cell: 0.9 ± 0.2 nA; $n = 6$ pairs; $P < 0.001$) (Fig. 6*C*–*E*). Despite a smaller fast EPSC amplitude (Fig. 6*C*, inset), mitral cells had an ∼5-fold larger synaptic charge compared to external tufted cells (synaptic charge at 100 V: mitral cell: 120.5 ± 14.9 pC; external tufted cell: 29.3 ± 6.6 pC; $P < 0.001$) (Fig. 6*C*, *D* and *F*). It is worth noting that the synaptic responses did not saturate, suggesting submaximal stimulation of ORN fibres using the theta electrode. There was no significant difference in the synaptic latency between mitral cells and external tufted cells at either high intensity (100 V; ETC: 1.02 ± 0.2 ms; MC: 1.5 ± 0.4 ms, $n = 6$ pairs; $P = 0.12$) or low intensity (10 V; ETC: 1.2 ± 0.2 ms; MC: 1.3 ± 0.09 ms, $n = 6$ pairs; $P = 0.96$). Low stimulation intensities failed to produce unitary EPSC events, presumably as a result of the high density of ORN fibres in any given bundle; however, unitary events were elicited in later experiments by desynchronizing release with strontium.

To examine the afferent evoked spiking patterns in both cell types, responses were recorded in current clamp. Cells were injected with bias current (usually <200 pA) to maintain a holding potential of −60 ± 5 mV. Consistent with the higher synaptic charge, brief afferent stimulation in current clamp recordings generated significantly more spikes in mitral cells (Fig. 7*A*). At maximal stimulation intensity, ORN stimulation produced 10.5 ± 3.5 action potentials in mitral cells compared to 4.0 ± 1.6 in external tufted cells ($P < 0.001$, $n = 6$ pairs). This trend persisted across stimulation intensities but was only statistically significant >10 V (Fig. 7*A* and *B*). There was no significant difference in the first spike latency between cell types at

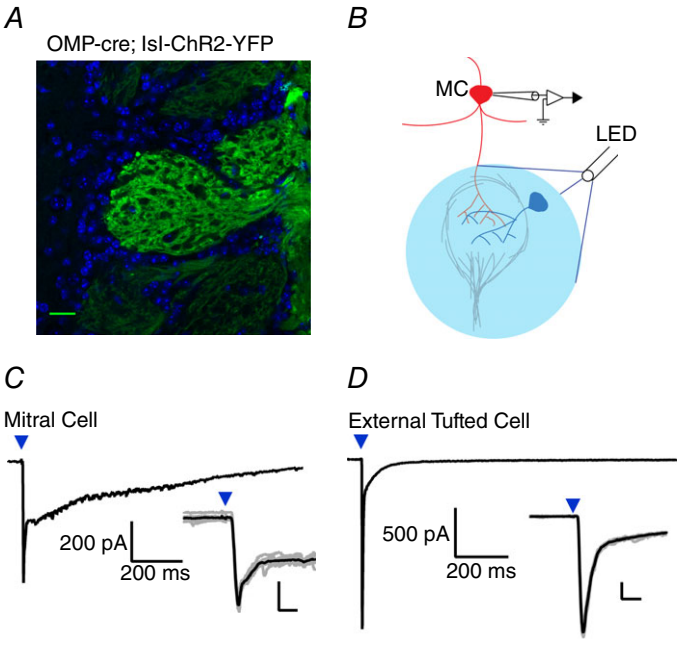

Figure 4. Optogenetic activation of ORNs elicits monosynaptic currents in mitral cells and external tufted cells
A, confocal image demonstrating expression of ChR2 in olfactory receptor neurons (green). Cell bodies are stained with 4′,6-diamidino-2-phenylindole and are shown in blue. *B*, schematic illustrating LED illumination (488 nm light, 2 ms widefield LED illumination; 15 mW mm^{-2}) centered on the innervated glomerulus. *C*, in mitral cells, 2 ms LED (denoted by blue arrowhead) illumination elicited a biphasic EPSC with a prominent fast component. The synaptic latency was 5.2 ± 0.17 ms and the jitter was 0.2 ± 0.03 ms, suggesting monosynaptic connectivity. Inset: overlay of raw traces (grey) and average (black) showing the fast peak of the optically evoked EPSC in mitral cells. *D*, in external tufted cells, LED stimulation also elicited a fast EPSC. The synaptic latency was 5.0 ± 0.47 ms and the synaptic jitter was 0.2 ± 0.04 ms. Inset: overlay of raw traces (grey) and average (black) showing the fast peak of the optically evoked EPSC in external tufted cells. Scale bar = 25 μm, Inset: 200 pA, 10 ms. [Colour figure can be viewed at wileyonlinelibrary.com]

maximal stimulation intensity (mitral cell: 2.7 ± 0.78 ms; external tufted cell: 2.4 ± 0.4 ms; $P = 0.78$, $n = 6$ pairs) or at low stimulation intensity (10 V; mitral cells: 3.7 ± 0.7 ms; external tufted cells: 3.3 ± 0.8 ms; $P = 0.21$, $n = 6$ pairs).

Because Cx36 gap junctions in apical dendrites are required for dendritic glutamate release (Christie *et al.* 2005; Christie and Westbrook, 2006; Maher *et al.* 2009), we used Cx36$^{-/-}$ animals to examine the impact of the slow EPSC on mitral and external tufted cell responses. In mitral cells from Cx36$^{-/-}$ animals, ORN stimulation produced a fast EPSC (Fig. 8*A*), which completely lacked the typical slow phase, reducing the total charge transfer (WT: 99.2 ± 23.8 pC, $n = 8$ cells; Cx36$^{-/-}$: 14.0 ± 0.8 pC, $n = 9$ cells; $P = 0.002$) (Fig. 8*A* and *B*) and shortening the EPSC duration accordingly (WT: 1014.1 ± 126.5 ms; Cx36$^{-/-}$: 26.7 ± 3.1 ms; $P < 0.0001$) (Fig. 8*A* and *C*). In external tufted cells from Cx36$^{-/-}$ mice the total charge transfer was also reduced (WT: 26.4 ± 8.1 pC, $n = 6$ cells; Cx36$^{-/-}$ 8.8 ± 0.4 pC, $n = 7$ cells; $P = 0.04$) (Fig. 8*D* and

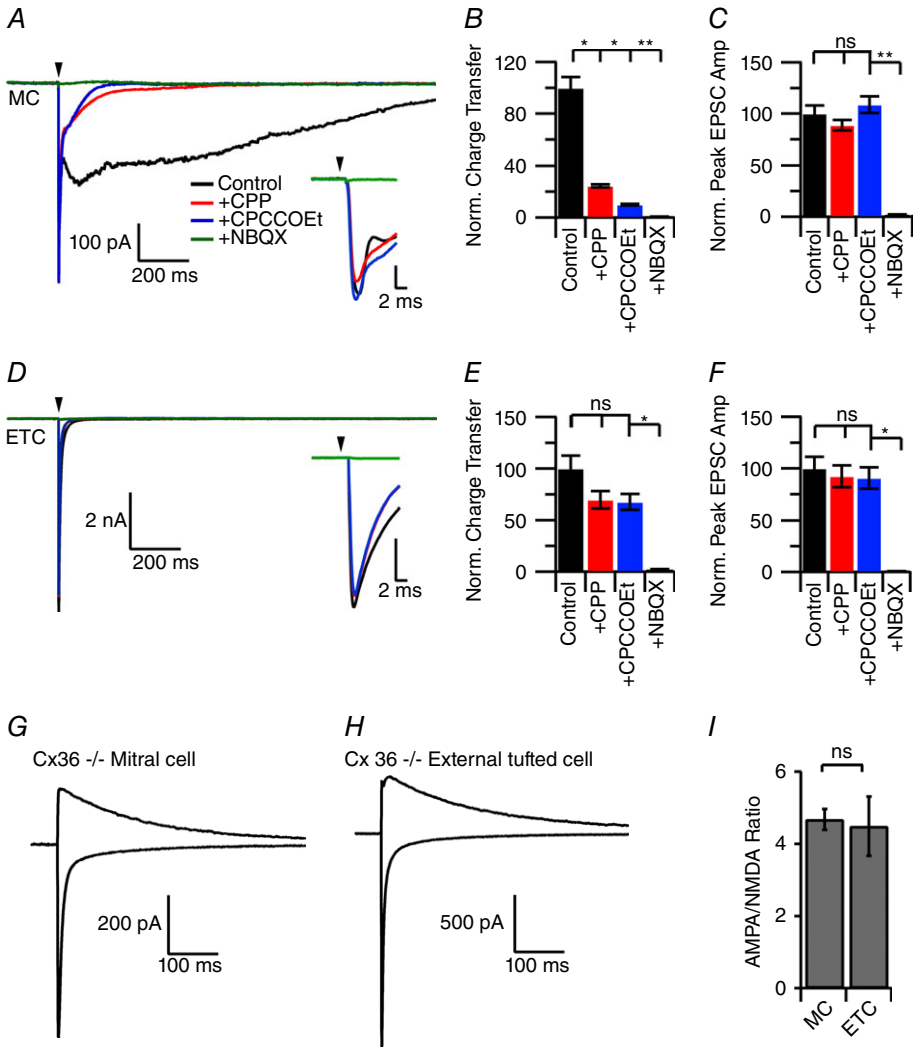

Figure 5. Pharmacology of the slow phase EPSC
A, under control conditions, brief afferent stimulation elicited a biphasic, prolonged EPSC in mitral cells. The majority of the slow component was blocked by the NMDA receptor antagonist CPP, and further reduced by the sequential addition of the mGluR1 receptor antagonist CPCCOEt. Bath application of NBQX abolished the fast component of the EPSC. *B*, quantification of the synaptic charge transfer across drug conditions demonstrates the block of the slow EPSC component by NMDA and mGluR1 receptor antagonists. *C*, neither CPP, nor CPCCOEt altered the peak EPSC amplitude. *D*, brief afferent stimulation elicited a fast EPSC in external tufted cells. *E*, unlike mitral cells, bath application of CPP and CPCCOEt had no significant effect on the synaptic charge. *F*, as in mitral cells, CPP and CPCCOEt did not reduce the peak EPSC amplitude. *G* and *H*, AMPA/NMDA ratio recorded from mitral cells (*G*) and external tufted cells (*H*) from Cx36$^{-/-}$ animals to isolate the ORN to principal neuron synapse. *I*, no significant difference in the AMPA/NMDA ratio between mitral and external tufted cells. [Colour figure can be viewed at wileyonlinelibrary.com]

E) without a significant change in the EPSC duration (WT: 27.7 ± 6.9 ms; Cx36$^{-/-}$: 16.88 ± 2.2; $P = 0.14$) (Fig. 7*D* and *F*). The impact of the Cx36$^{-/-}$ on the peak amplitude of the EPSC was quite variable. The peak ESPC amplitude appeared to be larger in mitral cells but did not reach statistical significance (WT: 374.5 ± 75.8 pA; Cx36$^{-/-}$: 629.0 ± 132.32 pA; $P = 0.13$). However, in external tufted cells, there was a decrease in the peak EPSC amplitude (WT: 3.2 ± 1.0 nA; Cx36$^{-/-}$: 1.3 ± 0.2 nA; $P = 0.04$). These differences may result from changes in shunting inhibition in the circuit lacking gap junctions. In current clamp, elimination of the slow component in Cx36$^{-/-}$ mice made the mitral cell spiking phenotype very similar to external tufted cells, producing at most one or two action potentials even at maximal stimulation intensities (WT: 10.5 ± 3.5 action potentials, $n = 5$ cells; Cx36$^{-/-}$: 1.7 ± 0.8, $n = 7$ cells; $P = 0.016$) (Fig. 8*G*–*I*). These results indicate that the monosynaptic current in mitral cells is sufficient

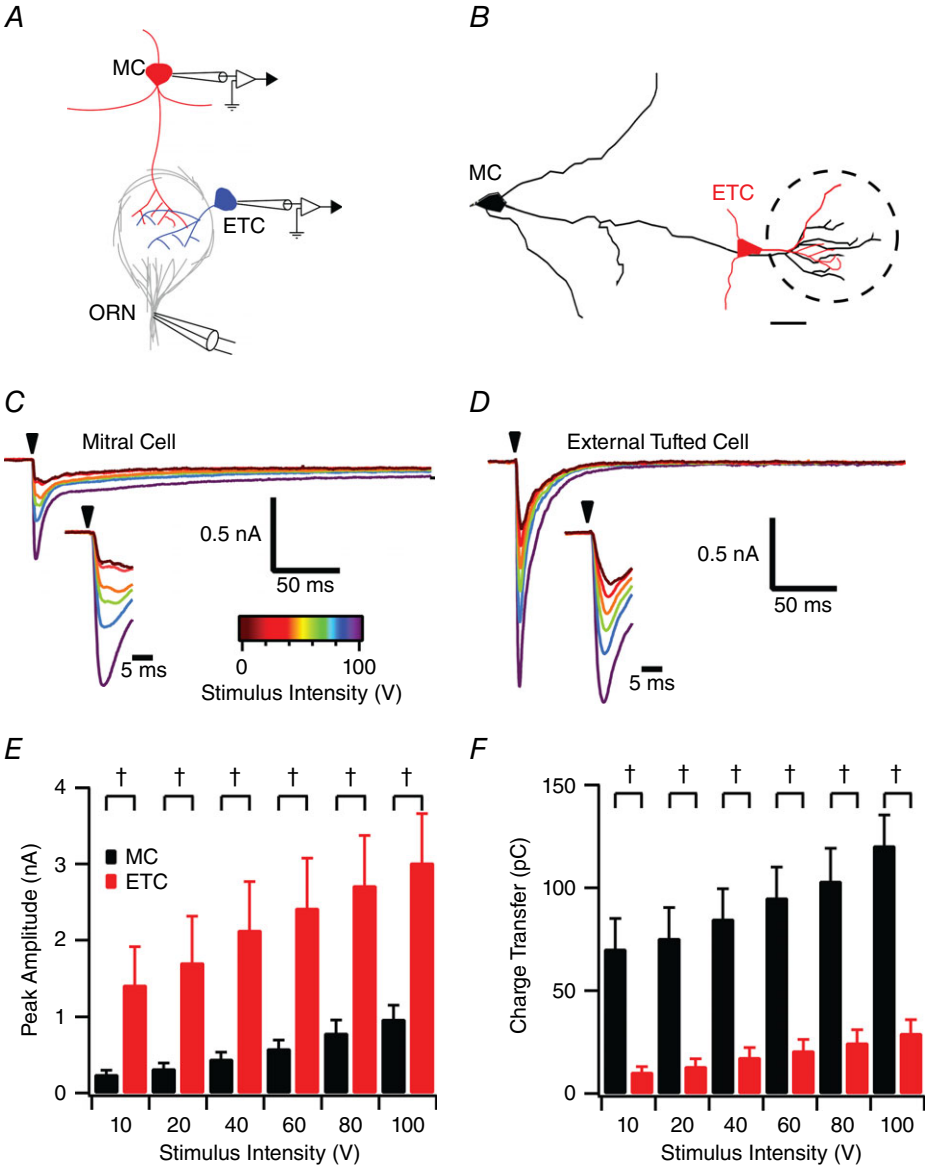

Figure 6. Paired recording comparison of afferent stimulation in mitral cells and external tufted cells
A, schematic of recording configuration: paired recordings were obtained from mitral cells and external tufted cells projecting to the same glomerulus (confirmed with Alexa-594 dye fill) and stimulated with a theta electrode. *B*, skeletal reconstruction of cell fills of a typical paired recording. *C* and *D*, mitral cell (*C*) and external tufted cell (*D*) EPSCs evoked by ORN stimulation. *E*, comparison of peak EPSC amplitudes between cell types across stimulus intensities. Across all stimulus intensities, external tufted cells had a larger peak EPSC amplitude (†$P < 0.0001$). *F*, conversely, mitral cells had a larger synaptic charge across all stimulus intensities, reflecting the slow EPSC component unique to mitral cells. Scale bar = 20 μm. [Colour figure can be viewed at wileyonlinelibrary.com]

to drive both synaptic responses and action potentials, but the slow component dramatically boosts generation of action potentials in mitral cells.

Comparing presynaptic properties

Given the different properties of mitral and external tufted cell responses to afferent stimulation, we examined possible presynaptic mechanisms using paired recordings of mitral and external cells. It is well established that the ORN is a high release probability synapse (Murphy *et al.* 2004). As expected, both cell types depressed with paired pulse stimulation (100 ms interstimulus interval, 2 mM Ca^{2+}, paired pulse ratio: mitral cells: 0.5 ± 0.05, external tufted cells: 0.6 ± 0.04; $P = 0.11$; $n = 6$ pairs) (Fig. 9*A*). Reducing the external Ca^{2+} to 1.5 mM similarly attenuated the EPSC amplitude in mitral and external tufted cells (mitral cell: 50.7 ± 4.6% of control; external tufted cell: 56.1 ± 5.0% of control; $P = 0.37$) (Fig. 9*A* and *B*) and increased the paired pulse ratio in parallel (mitral cell: 0.6 ± 0.05; external tufted cell: 0.7 ± 0.03; Holm-Sidak *post hoc* comparisons (2 mM: 1.5 mM Ca^{2+}) mitral cell: $P < 0.01$; external tufted cell: $P < 0.01$; $n = 6$ pairs) (Fig. 9*A* and *C*). The reduction in calcium increased the paired pulse ratio by 126.6 ± 5.4% in mitral cells and by 119.4 ± 4.15% in external tufted cells ($P = 0.31$). Thus, afferent inputs onto mitral and external tufted cells have similar release probabilities.

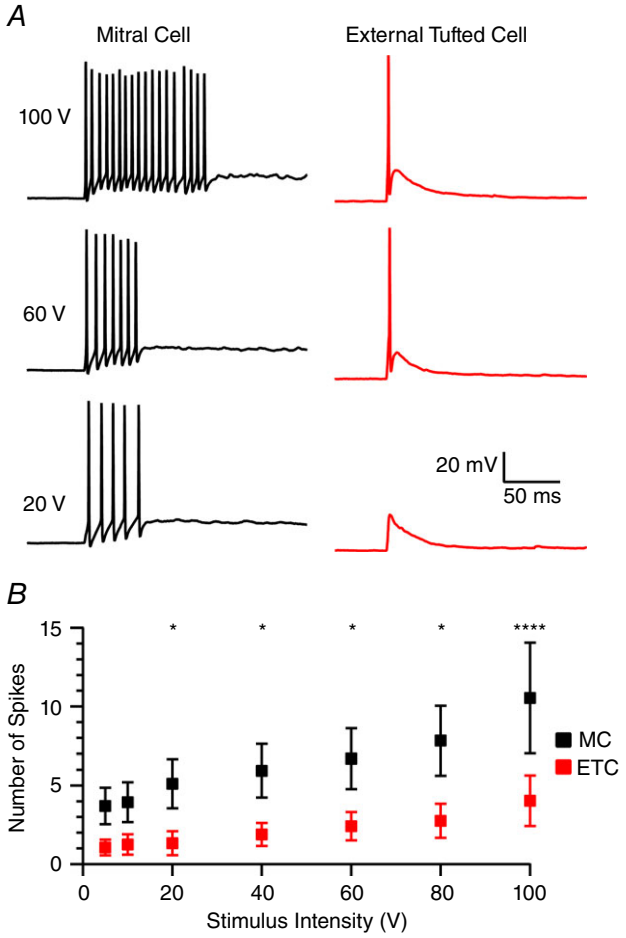

Figure 7. Slow mitral cell EPSC results in an increased spiking in response to afferent stimulation
A, comparison of the spiking responses in mitral cell and external tufted cell across three stimulation intensities (100, 60 and 20 V). All cells were held at −60 ± 5 mV with a bias current to isolate the synaptically evoked spiking responses. *B*, quantification of average number of action potentials as a function of cell type and stimulus intensity. At stimulation intensities >10 V, mitral cells produced significantly more action potentials than external tufted cells. [Colour figure can be viewed at wileyonlinelibrary.com]

Given the similar release probabilities, the larger fast EPSC amplitude in external tufted cells could result from differences in quantal amplitude or number of synaptic contacts. To test this, we isolated quantal events originating from the afferent nerve terminal, using $Cx36^{-/-}$ mice (Christie *et al.* 2005; Christie and Westbrook, 2006; Maher *et al.* 2009). Asynchronous release events, representing quantal release, were elicited by replacing external calcium with strontium to desynchronize vesicle release (Xu-Friedman and Regehr, 1999; Xu-Friedman and Regehr, 2000; Babai *et al.* 2014; Williams *et al.* 2015). Application of strontium (3 mM Sr^{2+};2 mM Mg^{2+}) reduced the fast EPSC amplitude and resulted in asynchronous EPSCs (Fig. 10*A*). As shown in Fig. 10, the asynchronous EPSC amplitude histograms were not normally distributed; therefore, non-parametric analyses were utilized. There was no significant difference in median quantal amplitude between mitral cells (29.9 pA, $n = 4$ cells, 395 events) and external tufted cells (30.8 pA, $n = 4$ cells, 624 events, Mann–Whitney test: $P = 0.054$) (Fig. 10*B*). Mitral cells had a slightly slower decay (mitral cell: 2.3 ± 0.02 ms; external tufted cell: 1.4 ± 0.3 ms; $P = 0.03$) probably as a result of dendritic filtering and reduced space clamp of the apical dendrite in mitral cells. Given the similar release probabilities and quantal amplitudes, the larger EPSC amplitude in external tufted cells probably results from more synaptic contacts. Assuming that the release probability is 0.8 (Murphy *et al.* 2004), the average peak amplitude of a mitral cell EPSC with our stimulation conditions results from 38.4 ± 4.9 synaptic contacts compared to 59.3 ± 2.4 synaptic contacts for an external tufted cell.

Discussion

One view of the flow of afferent information into the olfactory system is that olfactory receptor neurons exclusively contact external tufted cells, which, in turn, feedforward onto mitral cells directly or via inhibitory interneurons, before projecting to cortical areas. Our

results suggest a circuit organization in which both mitral cells and external tufted cells receive monosynaptic afferent input but differentially respond to brief stimulation. Purely feedforward excitation of mitral cells (Gire and Schoppa, 2009; Gire *et al.* 2012) was only observed in our experiments when weak stimuli were applied to the olfactory nerve layer (i.e. with stimulation of only a few axons to a particular glomerulus). Given that, in mice, ~11,000 axons innervate a glomerulus and make ~18 synaptic contacts each (Halasz and Greer, 1993; Klenoff and Greer, 1998; Shepherd, 2004), it is probably not the case that only a few ORNs will be activated by odorants. Therefore, purely feedforward excitation is probably not the only means of activating mitral cells. Our data are in agreement with recent computational studies, which suggest that multiple, parallel input pathways accurately predict *in vivo* mitral cell response properties (Carey *et al.* 2015).

Defining single glomerular inputs

It has long been known that odorants or electrical stimulation of the olfactory nerve trigger responses in both mitral and external tufted cells (Carlson *et al.* 2000; Schoppa and Westbrook, 2001; Hayar *et al.* 2004; De Saint Jan and Westbrook, 2007; Griff *et al.* 2008; Gire and Schoppa, 2009; Najac *et al.* 2011; Fukunaga *et al.* 2012; Igarashi *et al.* 2012; Wachowiak *et al.* 2013). However, whether mitral cells receive functional monosynaptic input from the olfactory nerve has been controversial. Although initial ultrastructural studies in both the rat and mouse (Pinching and Powell, 1971*a*; White, 1973; Kosaka *et al.* 2001; Najac *et al.* 2011) observed synaptic structures between olfactory nerve axons and mitral cell dendrites, physiologically stimulating a monosynaptic current has yielded mixed results. Macroscopic, peri-threshold stimulation of the nerve fibre layer in olfactory bulb slices failed to elicit clear monosynaptic currents in

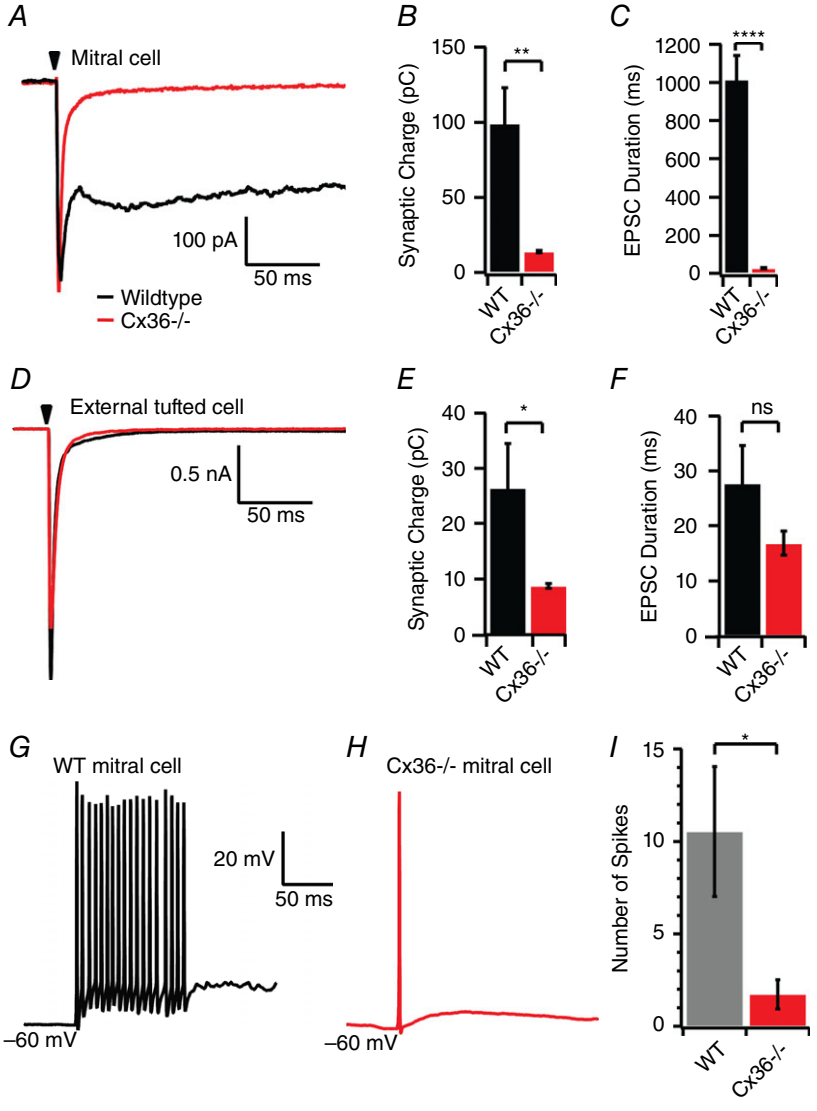

Figure 8. Synaptic responses in Cx-36 knockout animals
A, mitral cell response in WT (black) and Cx36$^{-/-}$ animal (red) demonstrating vastly different kinetics and charge redistribution. In mitral cells, EPSCs evoked in Cx36$^{-/-}$ animals had smaller synaptic charge transfer (*B*) and a shorter EPSC duration (*C*). *D*, afferent evoked responses in external tufted cells from Cx36$^{-/-}$ animals. *E*, external tufted cells from Cx36$^{-/-}$ animals had reduced synaptic charge. *F*, there was no significant change in external tufted cell EPSC duration. *G* and *H*, current clamp recordings from mitral cells in WT (*G*) and Cx36$^{-/-}$ (*H*) animals. *I*, the loss of the slow current reduced the total number of spikes produced in mitral cells. [Colour figure can be viewed at wileyonlinelibrary.com]

mitral cells (Gire and Schoppa, 2009; Gire *et al.* 2012). However, given that entering axons coursing through the cribiform plate do not organize into glomerular-specific bundles until just prior to entering the glomerulus (Mombaerts *et al.* 1996), nerve layer stimulation inevitably results in stimulation of only a few axons innervating any given glomerulus, leading to weak activation of many glomeruli. Conversely, more focal stimulation techniques have revealed a direct monosynaptic current (De Saint Jan *et al.* 2009; Najac *et al.* 2011); however, direct electrical stimulation of dendritic glutamate release has been raised as a concern (Gire *et al.* 2012). Therefore, the nature of the synaptic connectivity between primary sensory neurons and projection neurons in the olfactory bulb has remained contentious. The results of the present study, as obtained using spatially restricted, single glomerulus stimulation, demonstrate that monosynaptic mitral cell currents can be elicited by ORN activation (De Saint Jan *et al.* 2009; Najac *et al.* 2011). These results confirm a circuit diagram in which mitral cells receive parallel direct and indirect input via the ORN and external tufted cells, respectively.

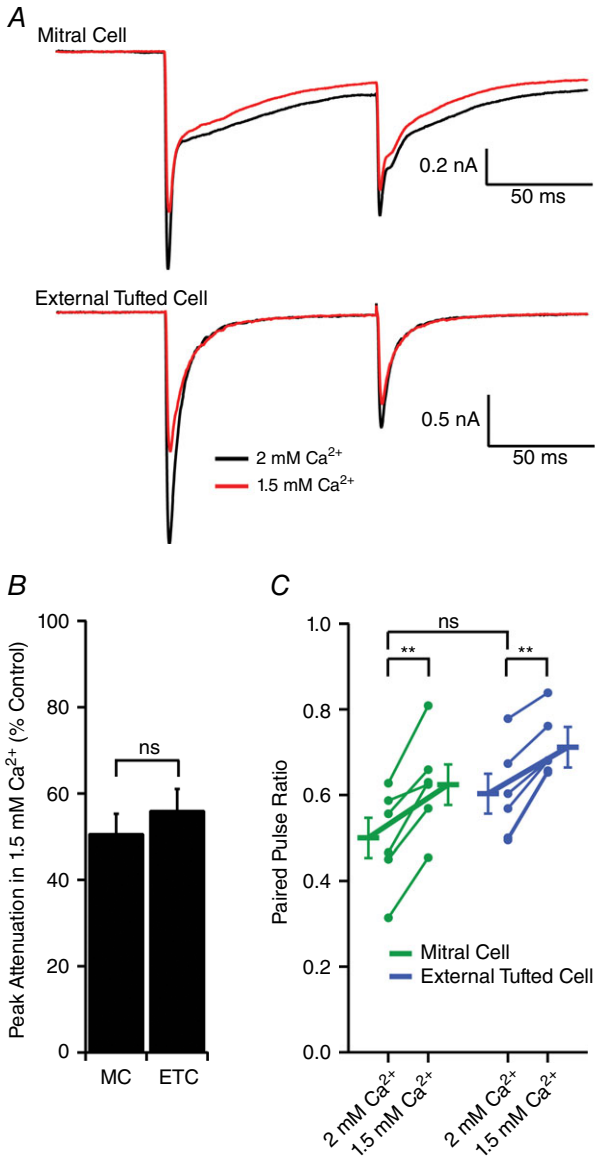

Figure 9. Homogeneous ORN release probability across cellular targets
A, paired recording from mitral cell and external tufted cell projecting to the same glomerulus. Paired stimuli (100 ms interval) elicited synaptic depression. Reducing the extracellular calcium from 2 mM to 1.5 mM similarly altered the paired pulse ratio in both cell types. *B*, reducing external calcium reduced the fast EPSC peak amplitude to the first stimulus in both mitral cells and external tufted cells. *C*, across pairs, there was no significant difference in the paired pulse ratio between cell types at 2 mM Ca^{2+}. However, decreasing external calcium similarly increased the paired pulse ratio in both cell types. [Colour figure can be viewed at wileyonlinelibrary.com]

A few apparent discrepancies with prior studies deserve discussion. The rationale for using peri-threshold stimulation in previous studies was that more direct stimulation of afferent nerve bundles entering individual glomeruli would inadvertently stimulate mitral and external tufted cell dendrites (Gire and Schoppa, 2009; Gire *et al.* 2012). Our results, however, clearly define the spatial spread of theta electrode stimulation, and preclude this possibility. Furthermore, Gire *et al.* (2012) suggested that mitral cell monosynaptic contacts, which they observed in $Cx36^{-/-}$ animals, are not functionally relevant because electrical coupling across mitral cell dendrites shunts the fast EPSC current. However, even at low stimulation intensities, mitral cells had a monosynaptic component that was sufficient to drive spiking, which is inconsistent with a purely feedforward activation mechanism. Gire *et al.* (2012) also reported predominantly slow currents in mitral cells using optogenetic techniques, however ChR2-mediated activation of ORNs in our experiments always included a monosynaptic component. These differences are probably explained by differences in the expression of ChR2, as well as the ChR2 variants used.

Taken together, these results suggest that mitral cells have two distinct activation patterns: a purely feedforward EPSC and a biphasic EPSC with a prominent monosynaptic response, both of which may be activated depending on the strength of the odorant. Although *in vivo*, sniff-activated odorant responses in mitral cells lag the responses in tufted cells (Fukunaga *et al.* 2012; Igarashi *et al.* 2012), these differences are on much slower time scales than either monosynaptic or disynaptic activation by afferents, and are probably a result of the efficacy of odour stimulation than the presence or absence of monosynaptic inputs to mitral cells. Furthermore, computational models in which ORNs form parallel direct and indirect inputs onto mitral cells accurately predict the *in vivo* response properties of mitral cells (Carey *et al.* 2015), which suggests that a parallel circuit arrangement is sufficient to explain the *in vivo* responses.

Comparing the response properties of mitral and external tufted cells

Our results confirm that both mitral cells and external tufted cells have monosynaptic components originating in the axodendritic shell of the glomerulus (Kasowski *et al.* 1999; Kim and Greer, 2000; De Saint Jan *et al.* 2009; Najac *et al.* 2011). However, the postsynaptic responses in these two pathways were quite different. The EPSC in mitral cells was 35-fold longer because of a slow synaptic current generated by dendritic glutamate release (Nicoll and Jahr, 1982; Carlson *et al.* 2000; Christie and Westbrook, 2006; De Saint Jan and Westbrook, 2007; Pimentel and Margrie, 2008; Najac *et al.* 2011), which was 4.5-fold larger in mitral cells. Why external tufted cells lack a more prominent slow current is unclear because their dendrites also occupy the core of the glomerulus, which contains the majority of dendrodendritic synapses (Pinching and Powell, 1971*b*; Kasowski *et al.* 1999; Kim and Greer, 2000; Kosaka and Kosaka, 2005). External tufted cell dendrites are also capable of releasing glutamate (Hayar *et al.* 2004; De Saint Jan *et al.* 2009; Najac *et al.* 2011) and can initiate slow currents in mitral cells (De Saint Jan *et al.* 2009). Classical dendrodendritic synapses between mitral cells and inhibitory granule cells are

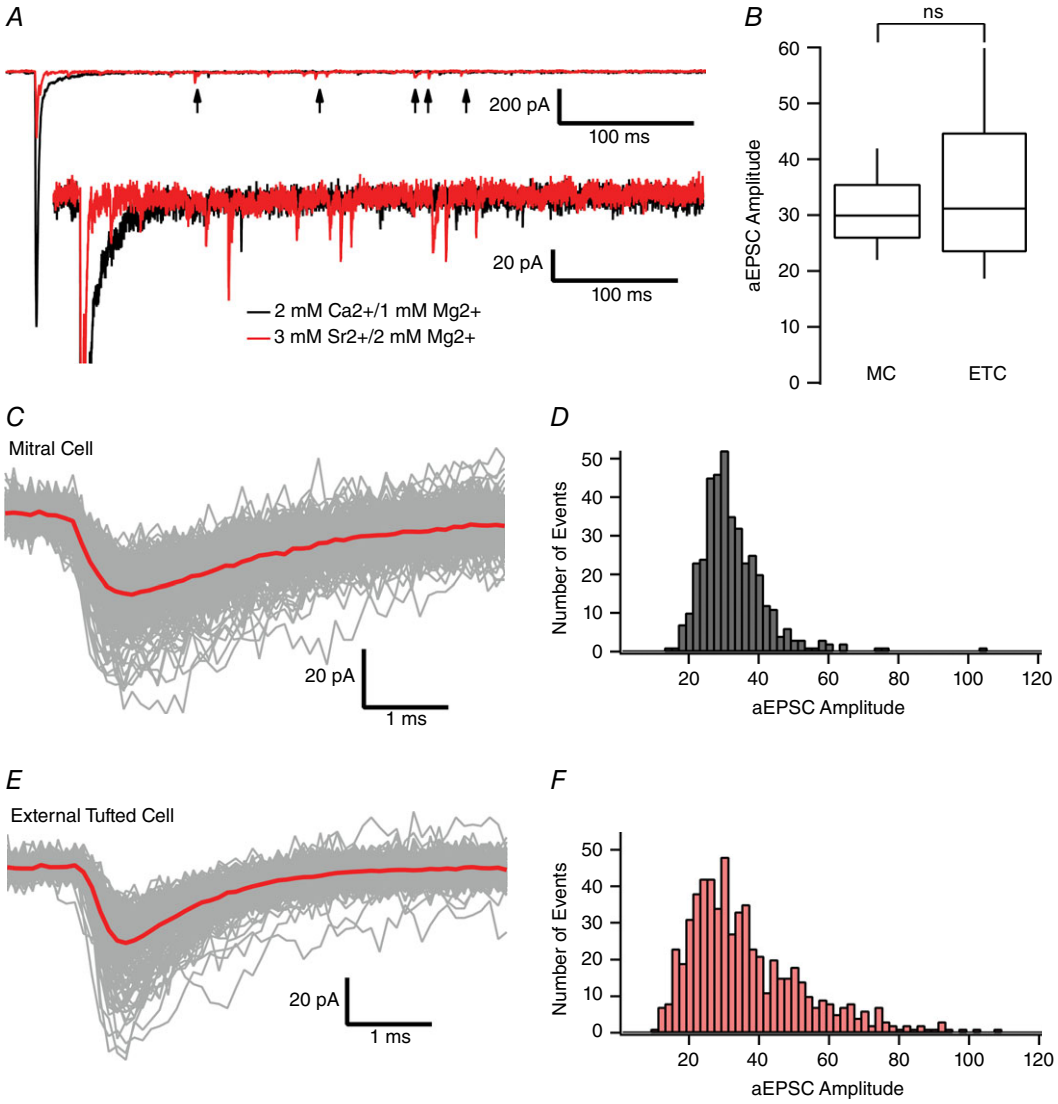

Figure 10. ORN synapses have similar quantal amplitudes in mitral cells and external tufted cells
A, example mitral cell recording from Cx36$^{-/-}$ animal to isolate ORN-evoked currents. Replacing extracellular calcium with 3 mM strontium (red trace) significantly reduced the fast, synchronous EPSC and resulted in asynchronous release events (arrows). *B*, comparison of asynchronous, quantal EPSCs recorded in mitral cells and external tufted cells. Raw traces (*C*) and histograms (*D*) of collected asynchronous EPSCs in mitral cells. Slower EPSC kinetics reflects dendritic filtering. Raw traces (*E*) and histograms (*F*) of collected asynchronous EPSCs in external tufted cells. [Colour figure can be viewed at wileyonlinelibrary.com]

reciprocal (Nowycky *et al.* 1981; Jahr and Nicoll, 1982; Schoppa *et al.* 1998; Isaacson and Strowbridge, 1998; Bartel *et al.* 2015). However, defining excitatory dendrodendritic synapses as reciprocal is difficult because vesicles are not clustered around discrete active zones and, instead, are dispersed along the dendrite (Pinching and Powell, 1971*a*). Indeed, in paired recordings, De Saint Jan *et al.* (2009) demonstrated that action potentials in external tufted cells could drive dendrodendritic EPSCs in mitral cells, although mitral cells were unable to drive EPSCs in external tufted cells, suggesting a unidirectional interaction. Functionally, external tufted cells potently activate inhibitory juxtaglomerular interneurons (Hayar *et al.* 2004; De Saint Jan *et al.* 2009; Najac *et al.* 2011); therefore, the brief time course of activation probably contributes to co-ordination of inhibitory neurons within the circuit.

Despite differences in postsynaptic responses, presynaptic release properties onto mitral cells and external tufted cells were similar. This pattern is perhaps not surprising because olfactory receptor neurons primarily serve as relays between the sensory epithelium and the olfactory bulb, as reflected, for example, in their high turnover rate, simple complement of ion channels and high transmitter release probability (Graziadei and Monti-Graziadei, 1979; Simmons and Getchell, 1981; Trombley and Westbrook, 1991; Murphy *et al.* 2004). Whether natural stimuli alter the presynaptic properties in these two principal cells has not been examined. Olfactory receptor neurons respond to natural odorants with high frequency bursts of action potentials (Gesteland and Sigwart, 1977; Getchell and Shepherd, 1978; Sicard, 1986; Duchamp-Viret, 1999; Savinger *et al.* 2009; Tan *et al.* 2010; Martelli *et al.* 2013), which probably reduces the effective release probability as a result of synaptic depression. For example, auditory nerve fibres have a high initial release probability; however, natural stimulation patterns engage both pre- and post-synaptic depression (Zhang and Trussell, 1994; Borst and Sakmann, 1996; Oleskevich *et al.* 2000). Given the exclusively monosynaptic responses in external tufted cells, it might be expected that synaptic depression would preferentially affect external tufted cell activation more than mitral cell activation.

Mitral and external tufted cells as parallel input pathways

The different response properties between mitral and external tufted cells suggest that these two principal neurons serve as distinct, but parallel, input pathways. It has been suggested that tufted cells serve as a labelled line, encoding odorant identity (Nagayama *et al.* 2010; Fukunaga *et al.* 2012; Igarashi *et al.* 2012). This hypothesis is supported by *in vivo* experiments suggesting that tufted cells fire earlier in the sniff cycle, respond to lower odorant concentrations and have more consistent responses across odorant concentrations (Fukunaga *et al.* 2012; Igarashi *et al.* 2012; Kikuta *et al.* 2013). Furthermore, tufted cells *in vivo* have higher odorant evoked firing rates than mitral cells (Nagayama *et al.* 2004; Griff *et al.* 2008). However, mitral cells have a more narrowly tuned molecular receptive range resulting from stronger afferent-evoked disynaptic inhibition (Shao *et al.* 2012; Kikuta *et al.* 2013), which may allow more effective discrimination between qualitatively similar odorants.

Although external tufted cells have been primarily viewed as local excitatory interneurons, recent evidence suggests that they do project to higher areas of cortex (Nagayama *et al.* 2010; Igarashi *et al.* 2012). Interestingly, mitral cells and external tufted cells (indeed, all tufted cells) project to distinct, non-overlapping regions of olfactory cortex (Nagayama *et al.* 2010; Igarashi *et al.* 2012), suggesting discrete functions in higher olfactory processing. Mitral cells project broadly to the piriform cortex, entorhinal cortex and amygdala, whereas external tufted cells make extensive local connections within the glomerulus and project to much more circumscribed regions of the anterior piriform cortex and anterior olfactory nucleus (Hayar *et al.* 2004; De Saint Jan 2009; Kiyokage *et al.* 2010; Nagayama *et al.* 2010; Najac *et al.* 2011; Igarashi *et al.* 2012).

The robust amplification of brief afferent input in mitral cells compared to the transient response profile of external tufted cells is consistent with the view that mitral cells are important for odorant discrimination. This distinction may be even more pronounced with natural ORN stimulation patterns (Duchamp-Viret, 1999; Savinger *et al.* 2009; Tan *et al.* 2010). Overall, our results suggest that large transient response of external tufted cells is well positioned to encode the presence of an odorant, and engage glomerular interneurons via feed-forward excitation. Conversely, the robust amplification of brief afferent input by mitral cells is well suited to most effectively drive activity in downstream cortical areas.

References

Aroniadou-Anderjaska V, Ennis M & Shipley MT (1999). Dendrodendritic recurrent excitation in mitral cells of the rat olfactory bulb. *J Neurophys* **82**, 489–494.

Babai N, Kochubey O, Keller D & Schneggenburger R (2014). An alien divalent ion reveals a major role for Ca^{2+} buffering in controlling slow transmitter release. *J Neurosci* **34**, 12622–12635.

Bartel DL, Rela L, Hsieh L & Greer CA (2015). Dendrodendritic synapses in the mouse olfactory bulb external plexiform layer. *J Comp Neurol* **523**, 1145–1161.

Berry MS & Pentreath VW (1976). Criteria for distinguishing between monosynaptic and polysynaptic transmission. *Brain Res* **105**, 1–20.

Borisovska M, McGinley MJ, Bensen A & Westbrook GL (2011). Loss of olfactory cell adhesion molecule reduces the synchrony of mitral cell activity in olfactory glomeruli. *J Physiol* **589**, 1927–1941.

Borst JGG & Sakmann B (1996). Calcium influx and transmitter release in a fast CNS synapse. *Nature* **383**, 431–434.

Buck L & Axel R (1991). A novel multigene family may encode odorant receptors: a molecular basis for odor recognition. *Cell* **65**, 175–187.

Carey RM, Sherwood WE, Shipley MT, Borisyuk A & Wachowiak M (2015). Role of intraglomerular circuits in shaping temporally structured responses to naturalistic inhalation-driven sensory input to the olfactory bulb. *J Neurophys* **113**, 3112–3129.

Carlson GC, Shipley MT & Keller A (2000). Long-lasting depolarizations in mitral cells of the rat olfactory bulb. *J Neurosci* **20**, 2011–2021.

Christie JM, Bark C, Hormuzdi SG, Helbig I, Monyer H & Westbrook GL (2005). Connexin36 mediates spike synchrony in olfactory bulb glomeruli. *Neuron* **46**, 761–772.

Christie JM, Schoppa NE & Westbrook GL (2001). Tufted cell dendrodendritic inhibition in the olfactory bulb is dependent on NMDA receptor activity. *J Neurophys* **85**, 169–173.

Christie JM & Westbrook GL (2006). Lateral excitation within the olfactory bulb. *J Neurosci* **26**, 2269–2277.

De Saint Jan D, Hirnet D, Westbrook GL & Charpak S (2009). External tufted cells drive the output of olfactory bulb glomeruli. *J Neurosci* **29**, 2043–2052.

De Saint Jan D & Westbrook GL (2007). Disynaptic amplification of metabotropic glutamate receptor 1 responses in the olfactory bulb. *J Neurosci* **27**, 132–140.

Duchamp-Viret P, Chaput MA & Duchamp A (1999). Odor response properties of rat olfactory receptor neurons. *Science* **284**, 2171–2174.

Feng G, Mellor RH, Bernstein M, Keller-Peck C, Nguyen QT, Wallace M, Nerbonne JM, Lichtman JW & Sanes JR (2000). Imaging neuronal subsets in transgenic mice expressing multiple spectral variants of GFP. *Neuron* **28**, 41–51.

Friedman D & Strowbridge BW (2000). Functional role of NMDA autoreceptors in olfactory mitral cells. *J Neurophys* **84**, 39–50.

Fukunaga I, Berning M, Kollo M, Schmaltz A & Schaefer AT (2012). Two distinct channels of olfactory bulb output. *Neuron* **75**, 320–329.

Gesteland RC & Sigwart CD (1977). Olfactory receptor units – a mammalian preparation. *Brain Res* **133**, 144–149.

Getchell TV & Shepherd GM (1978). Responses of olfactory receptor cells to step pulses of odour at different concentrations in the salamander. *J Physiol* **282**, 521–540.

Gire DH, Franks KM, Zak JD, Tanaka KF, Whitesell JD, Mulligan AA, Hen R & Schoppa NE (2012). Mitral cells in the olfactory bulb are mainly excited through a multistep signaling path. *J Neurosci* **32**, 2964–2975.

Gire DH & Schoppa NE (2009). Control of on/off glomerular signaling by a local GABAergic microcircuit in the olfactory bulb. *J Neurosci* **29**, 13454–13464.

Graziadei PPC & Monti-Graziadei GA (1979). Neurogenesis and neuron regeneration in the olfactory system of mammals. I. Morphological aspects of differentiation and structural organization of the olfactory sensory neurons. *J Neurocytol* **8**, 1–18.

Griff ER, Mafhouz M & Chaput MA (2008). Comparison of identified mitral and tufted cells in freely breathing rats: II. Odor-evoked responses. *Chem Senses* **33**, 793–802.

Halasz N & Greer CA (1993). Terminal arborizations of olfactory nerve fibers in the glomeruli of the olfactory bulb. *J Comp Neurol* **337**, 307–316.

Hayar A, Karnup S, Ennis M & Shipley MT (2004). External tufted cells: a major excitatory element that coordinates glomerular activity. *J Neurosci* **24**, 6676–6685.

Igarashi KM, Ieki N, An M, Yamaguchi Y, Nagayama S, Kobayakawa K, Kobayakawa R, Tanifuji M, Sakano H, Chen WR & Mori K (2012). Parallel mitral and tufted cell pathways route distinct odor information to different targets in the olfactory cortex. *J Neurosci* **32**, 7970–7985.

Isaacson JS (1999). Glutamate spillover mediates excitatory transmission in the rat olfactory bulb. *Neuron* **23**, 377–384.

Isaacson JS & Strowbridge BW (1998). Olfactory reciprocal synapses: dendritic signaling in the CNS. *Neuron* **20**, 749–761.

Jahr CE & Nicoll RA (1982). An intracellular analysis of dendrodendritic inhibition in the turtle in vitro olfactory bulb. *J Physiol* **326**, 213–234.

Kasowski HJ, Kim H & Greer CA (1999). Compartmental organization of the olfactory bulb glomerulus. *J Comp Neurol* **407**, 261–274.

Kikuta S, Fletcher ML, Homma R, Yamasoba T & Nagayama S (2013). Odorant response properties of individual neurons in an olfactory glomerular module. *Neuron* **77**, 1122–1135.

Kim H & Greer CA (2000). The emergence of compartmental organization in olfactory bulb glomeruli during postnatal development. *J Comp Neurol* **422**, 297–311.

Kiyokage E, Pan Y-Z, Shao Z, Kobayashi K, Szabo G, Yanagawa Y, Obata K, Okano H, Toida K, Puche AC & Shipley MT (2010). Molecular identity of periglomerular and short axon cells. *J Neurosci* **30**, 1185–1196.

Klenoff JR & Greer CA (1998). Postnatal development of olfactory receptor cell axonal arbors. *J Comp Neurol* **390**, 256–267.

Kosaka K, Aika Y, Toida K & Kosaka T (2001). Structure of intraglomerular dendritic tufts of mitral cells and their contacts with olfactory nerve terminals and calbindin-immunoreactive type 2 periglomerular neurons. *J Comp Neurol* **440**, 219–235.

Kosaka K & Kosaka T (2005). Synaptic organization of the glomerulus in the main olfactory bulb: compartments of the glomerulus and heterogeneity of the periglomerular cells. *Anat Sci Int* **80**, 80–90.

Maher BJ, McGinley MJ & Westbrook GL (2009). Experience-dependent maturation of the glomerular microcircuit. *Proc Natl Acad Sci USA* **106**, 16865–16870.

Martelli C, Carlson JR & Emonet T (2013). Intensity invariant dynamics and odor-specific latencies in olfactory receptor neuron response. *J Neurosci* **33**, 6285–6297.

Mombaerts P, Wang F, Dulac C, Chao SK, Nemes A, Mendelsohn M, Edmondson J & Axel R (1996). Visualizing an olfactory sensory map. *Cell* **87**, 675–686.
Mori K, Nagao H & Yoshihara Y (1999). The olfactory bulb: coding and processing of odor molecule information. *Science* **286**, 711–715.
Murphy GJ, Glickfeld LL, Balsen Z & Isaacson JS (2004). Sensory neuron signaling to the brain: properties of transmitter release from olfactory nerve terminals. *J Neurosci* **24**, 3023–3030.
Nagayama S, Enerva A, Fletcher ML, Masurkar AV, Igarashi KM, Mori K & Chen WR (2010). Differential axonal projection of mitral and tufted cells in the mouse main olfactory system. *Front Neural Circuits* **4**, 120.
Nagayama S, Takahashi YK, Yoshihara Y & Mori K (2004). Mitral and tufted cells differ in the decoding manner of odor maps in the rat olfactory bulb. *J Neurophysiol* **91**, 2532–2540.
Najac M, De Saint Jan D, Reguero L, Grandes P & Charpak S (2011). Monosynaptic and polysynaptic feed-forward inputs to mitral cells from olfactory sensory neurons. *J Neurosci* **31**, 8722–8729.
Nicoll RA & Jahr CE (1982). Self-excitation of olfactory bulb neurones. *Nature* **296**, 441–444.
Nowycky MC & Mori K (1981). GABAergic mechanisms of dendrodendritic synapses in isolated turtle olfactory bulb. *J Neurophysiol* **46**, 639–648.
Oleskevich S, Clements J & Walmsley B (2000). Release probability modulates short-term plasticity at a rat giant terminal. *J Physiol* **524**, 513–523.
Pimentel DO & Margrie TW (2008). Glutamatergic transmission and plasticity between olfactory bulb mitral cells. *J Physiol* **586**, 2107–2119.
Pinching AJ & Powell TP (1971*a*). The neuropil of the glomeruli of the olfactory bulb. *J Cell Sci* **9**, 347–377.
Pinching AJ & Powell TP (1971*b*). The neuron types of the glomerular layer of the olfactory bulb. *J Cell Sci* **9**, 305–345.
Ressler KJ, Sullivan SL & Buck LB (1994). Information coding in the olfactory system: Evidence for a stereotyped and highly organized epitope map in the olfactory bulb. *Cell* **79**, 1245–1255.
Rubin BD & Katz LC (1999). Optical imaging of odorant representations in the mammalian olfactory bulb. *Neuron* **23**, 499–511.
Savinger A, Duchamp-Viret P, Grosmaitre X, Chaput M, Garcia S, Ma M & Palouzier-Paulignan B (2009). Modulation of spontaneous and odorant-evoked activity in rat olfactory sensory neurons by two anorectic peptides, insulin and leptin. *J Neurophysiol* **101**, 2898–2906.
Schoppa NE, Kinzie JM, Sahara Y, Segerson TP & Westbrook GL (1998). Dendrodendritic inhibition in the olfactory bulb is driven by NMDA receptors. *J Neurosci* **18**, 6790–6802.
Schoppa NE & Westbrook GL (2001). Glomerulus-specific synchronization of mitral cells in the olfactory bulb. *Neuron* **31**, 639–651.
Shao Z, Puche AC, Liu S & Shipley MT (2012). Intraglomerular inhibition shapes the strength and temporal structure of glomerular output. *J Neurophys* **108**, 782–793.
Shepherd GM (2004). *The Synaptic Organization of the Brain*, 5th edn. Oxford University Press, Oxford.
Sicard G (1986). Electrophysiological recordings from olfactory receptor cells in adult mice. *Brain Res* **397**, 405–408.
Simmons PA & Getchell TV (1981). Neurogenesis in olfactory epithelium: loss and recovery of transepithelial voltage transients following olfactory nerve section. *J Neurophysiol* **45**, 516–528.
Tan J, Savinger A, Ma M & Luo M (2010). Odor information processing by the olfactory bulb analyzed in gene-targeted mice. *Neuron* **65**, 912–926.
Treloar HB, Feinstein P, Mombaerts P & Greer CA (2002). Specificity of glomerular targeting by olfactory sensory axons. *J Neurosci* **22**, 2469–2477.
Trombley PQ & Westbrook GL (1991). Voltage-gated currents in identified rat olfactory receptor neurons. *J Neurosci* **11**, 435–444.
Urban NN & Sakmann B (2002). Reciprocal intraglomerular excitation and intra- and interglomerular lateral inhibition between mouse olfactory bulb mitral cells. *J Physiol* **542**, 355–367.
Vassar R, Ngai J & Axel R (1993). Spatial segregation of odorant receptor expression in the mammalian olfactory epithelium. *Cell* **74**, 309–318.
Wachowiak M & Cohen LB (2001). Representation of odorants by receptor neuron input to the mouse olfactory bulb. *Neuron* **32**, 723–735.
Wachowiak M, Economo MN, Díaz-Quesada M, Brunert D, Wesson DW, White JA & Rothermel M (2013). Optical dissection of odor information processing in vivo using GCaMPs expressed in specified cell types of the olfactory bulb. *J Neurosci* **33**, 5285–5300.
White EL (1973). Synaptic organization of the mammalian olfactory glomerulus: new findings including an intraspecific variation. *Brain Res* **60**, 299–313.
Williams MR, DeSpenza T, Li M, Gulledge AT & Luikart BW (2015). Hyperactivity of newborn Pten knock-out neurons results from increased excitatory synaptic drive. *J Neurosci* **35**, 943–959.
Xu-Friedman MA & Regehr WG (1999). Presynaptic Strontium Dynamics and Synaptic Transmission. *Biophysical Journal* **76**, 2029–2042.
Xu-Friedman MA & Regehr WG (2000). Probing fundamental aspects of synaptic transmission with strontium. *J Neurosci* **20**, 4414–4422.
Zhang S & Trussell LO (1994). Voltage clamp analysis of excitatory synaptic transmission in the avian nucleus magnocellularis. *J Physiol* **480**, 123–136.

Additional information

Competing interests

The authors declare that they have no competing interests.

Author contributions

CEV and GLW were involved in the conception and design of the experiments. CEV and GLW were involved in the collection, assembly, analysis and interpretation of data.

CEV and GLW were involved in the drafting and revision of the article. Experiments were performed in the Westbrook lab at the Vollum Institute, Oregon Health and Science University.

Funding

This work was supported by NS26494 (GLW), National Science Foundation Graduate Research Fellowship DGE-0925180 (CEV) and a P30 imaging grant (NS061800).

Acknowledgements

We thank the members of the Westbrook laboratory for their helpful comments. We also thank Dr Charles Greer for the Thy1-eYFP transgenic mice.